FOCUS: ION-SURFACE COLLISIONS AND PEPTIDE RADICAL CATIONS

Experimental and Computational Studies of the Macrocyclic Effect of an Auxiliary Ligand on Electron and Proton Transfers Within Ternary Copper(II)–Histidine Complexes

Tao Song,[a] Corey N. W. Lam,[a] Dominic C. M. Ng,[a] Galina Orlova,[b]
Julia Laskin,[c] De-Cai Fang,[d] and Ivan K. Chu[a]

[a] Department of Chemistry, The University of Hong Kong, Pokfulam Road, Hong Kong, China
[b] Department of Chemistry, St. Francis Xavier University, Antigonish, NS, Canada, B2G 2W5
[c] Pacific Northwest National Laboratory, Fundamental Sciences Division, Richland, Washington, USA
[d] College of Chemistry, Beijing Normal University, China

The dissociation of $[Cu^{II}(L)His]^{\bullet 2+}$ complexes [L = diethylenetriamine (dien) or 1,4,7-triazacyclononane (9-aneN$_3$)] bears a strong resemblance to the previously reported behavior of $[Cu^{II}(L)GGH]^{\bullet 2+}$ complexes. We have used low-energy collision-induced dissociation experiments and density functional theory (DFT) calculations at the B3LYP/6-31+G(d) level to study the macrocyclic effect of the auxiliary ligands on the formation of His$^{\bullet +}$ from prototypical $[Cu^{II}(L)His]^{\bullet 2+}$ systems. DFT revealed that the relative energy barriers of the same electron-transfer (ET) dissociation pathways of $[Cu^{II}(9\text{-aneN}_3)His]^{\bullet 2+}$ and $[Cu^{II}(dien)His]^{\bullet 2+}$ are very similar, with the ET reactions of $[Cu^{II}(9\text{-aneN}_3)His]^{\bullet 2+}$ leading to the generation of two distinct His$^{\bullet +}$ species; in contrast, the proton transfer (PT) dissociation pathways of $[Cu^{II}(9\text{-aneN}_3)His]^{\bullet 2+}$ and $[Cu^{II}(dien)His]^{\bullet 2+}$ differ considerably. The PT reactions of $[Cu^{II}(9\text{-aneN}_3)His]^{\bullet 2+}$ are associated with substantially higher barriers (>13 kcal/mol) than those of $[Cu^{II}(dien)His]^{\bullet 2+}$. Thus, the sterically encumbered auxiliary 9-aneN$_3$ ligand facilitates ET reactions while moderating PT reactions, allowing the formation of hitherto nonobservable histidine radical cations. (J Am Soc Mass Spectrom 2009, 20, 972–984) © 2009 Published by Elsevier Inc. on behalf of American Society for Mass Spectrometry

Electron transfer (ET) is a fundamental process that has been studied extensively in inorganic, organic, and biological systems [1]. In most cases, a metal cofactor is mandatory if protein oxidation is to occur via an ET process [2–6]; nevertheless, the chemical mechanisms governing the formation of such protein radicals remain unclear. Oxidized radical products from Cu(II)–protein ion complexes have been proposed as intermediates that play key roles in several neurodegenerative conditions, including Alzheimer's disease (β-amyloid peptide) and bovine spongiform encephalitis (prion protein) [3, 4]. It was demonstrated recently that the dissociation of ligated Cu(II)–peptide complexes $[Cu^{II}(L)M]^{\bullet 2+}$ (L, ligand; M, peptide) generates peptide radical cations (M$^{\bullet +}$) through ET dissociation in the gas phase [7–18]. Such complexes are a useful simple system for studyi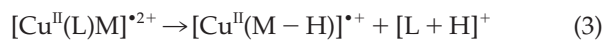ng the fundamental parameters that govern the formation of peptide radical cations through single-electron transfer in the absence of solvation.

$$[Cu^{II}(L)M]^{\bullet 2+} \rightarrow [Cu^{I}(L)]^{+} + M^{\bullet +} \qquad (1)$$
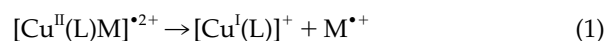
The collision-induced dissociation (CID) of ligated Cu(II)–peptide complexes is the simplest prototype available to elucidate the intrinsic properties of ET between ligated metal ions and peptides that are unencumbered by solvation. The experimental results can be further examined in conjunction with theoretical calculations. Several systematic studies have been performed to determine the roles played by the auxiliary ligands and metals during the formation of peptide radical cations through ET dissociation (Reaction 1) [7–16]. Three major competitive dissociation pathways have been reported: proton transfer (PT) to the peptide (Reaction 2) [7–12, 14, 16, 19–21], proton abstraction from the peptide (Reaction 3) [7, 8, 10, 11, 22], and peptide fragmentation (Reaction 4) [7–12, 14, 19, 20, 23, 24].

$$[Cu^{II}(L)M]^{\bullet 2+} \rightarrow [Cu^{II}(L-H)]^{\bullet +} + [M+H]^{+} \qquad (2)$$
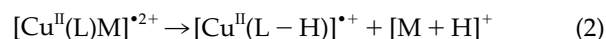
Address reprint requests to Dr. Ivan K. Chu, The University of Hong Kong, Department of Chemistry, Chong Yuet Ming Chemistry Building, Pokfulam Road, Hong Kong. E-mail: ivankchu@hkucc.hku.hk or to De-Cai Fang: E-mail: dcfang@bnu.edu.cn

$$[Cu^{II}(L)M]^{\bullet 2+} \rightarrow [Cu^{II}(M-H)]^{\bullet +} + [L+H]^+ \qquad (3)$$

$$[Cu^{II}(L)M]^{\bullet 2+} \rightarrow [Cu^{II}(L)(M-b_n)]^{\bullet +} + b_n^+ \qquad (4)$$

The nature of the auxiliary ligand in Cu(II) complexes is an important factor affecting the formation of peptide radical cations [12, 14–16]. Studies into the dissociation of $[Cu^{II}(dien)M]^{\bullet 2+}$ complexes (dien: diethylenetriamine) have indicated that ET reactions predominate only for peptides containing tryptophan or tyrosine residues, which have relatively low ionization energies; other peptides dissociate preferably through PT reactions, especially for peptides containing basic amino residues [7–9]. PT can be moderated by using ligands such as N,N,N',N',N''-pentamethyldiethylenetriamine (Me$_5$dien) and 2,2':6',2''-terpyridine (terpy). These systems are restricted, however, to peptides that contain either basic (lysyl, arginyl, or histidyl) or aromatic (tyrosyl or tryptophanyl) residues. For terpy-containing systems, facile peptide cleavage is a prominent reaction pathway that competes with peptide radical formation. The use of an auxiliary ligand that is more sterically encumbered [e.g., 6,6''-dibromo-2,2':6',2''-terpyridine, 1,4,7,10-tetraoxacyclododecane (12-crown-4), or 1,4,7-triazacyclononane (9-aneN$_3$)] results in ET reactions being further facilitated to such a degree that they can even generate aliphatic-only tripeptide radical cations [14–16]. The effects of macrocyclic auxiliary ligands and their acyclic analogues have been investigated previously through CID experiments on a series of GGX tripeptides having substantial differences in their proton affinities and ionization energies. In particular, replacing open-chain ligands (dien and triglyme) with their macrocyclic auxiliary ligand analogues (9-aneN$_3$ and 12-crown-4, respectively) has been demonstrated empirically to facilitate ET reactions (Reaction 1), while moderating other competitive reactions (Reactions 2–4). The enhancement in peptide radical cation formation on $[Cu^{II}(9\text{-}aneN_3)]^{\bullet 2+}$ seems surprising because the 9-aneN$_3$ and dien ligands share similar features (e.g., three amino donor atoms, NH hydrogen atoms). The effect of the sterically encumbered ligand is somewhat similar to that of the classical example of the entatic state of ligated Cu(II) ions in metalloproteins, in which a constrained ligated Cu(II) complex facilitates ET reactions [25–27]. Knowledge of the factors that control the formation of peptide radical cations will be of value for elucidating the phenomena that occur during ET processes within metalloproteins; it may also generate valuable new insights for the design of systems that allow the formation of peptide radical cations more efficiently. In fact, amino acid side chains are good endogenous biological ligands that facilitate ET reactions between transition-metal sites and peptides in metalloproteins.

Our interest in this phenomenon led us to further examine the dependence of the ET process on the structure of the auxiliary ligand during radical formation. The objective of this study was to use these prototypical systems to improve our fundamental understanding of ET and to explore the factors that govern the formation of peptide radical cations. In particular, we focused our efforts on the effects of macrocyclic auxiliary ligands on the competition between the ET and PT processes. To elucidate the mechanisms of peptide radical cation formation that arise from the macrocyclic effect of the auxiliary ligands, we attempted to further constrain the permanent non-zwitterionic structures of amino acids to rule out reactions arising from zwitterionic forms [17]. Our experimental approach involved maintaining the histidine fragment in its non-zwitterionic form within $[Cu^{II}(L)(His + OMe)]^{\bullet 2+}$ complexes, where His + OMe is the histidine methyl ester, which can exist only in its canonical (non-zwitterionic) form. The advantages of this experimental method are (1) that the ternary complex ions of interest can be readily produced, isolated, and probed using tandem mass spectrometry; and (2) that the experimental results can be examined in conjunction with theoretical calculations. Thus, we performed density functional theory (DFT) calculations of the major competitive reactions using $[Cu^{II}(dien)His]^{\bullet 2+}$ and its cyclic analogue $[Cu^{II}(9\text{-}aneN_3)His]^{\bullet 2+}$ as model systems. This prototypical system may shed light on our understanding of how the structures and conformations of metalloproteins influence the intrinsic ET processes occurring in biological systems.

Experimental

Materials

All chemicals were commercially available (Aldrich or Sigma, St. Louis, MO, USA; Bachem, King of Prussia, PA, USA). The Cu(II) dien and 9-aneN$_3$ complexes were prepared in situ by mixing 600 mM Cu(NO$_3$)$_2$ with 600 mM the ligand in a 50:50 water/MeOH solution.

Methylation of Peptides

An approximately 2 M solution of HCl in MeOH was prepared through the dropwise addition of acetyl chloride (800 μL) into anhydrous MeOH (5 mL) and then stirring for 5 min at room temperature. This solution (1 mL) was added to the peptide (10 mg) and then the mixture was stirred for 3 h at room temperature. The resulting solution was dried using a SC250DDA Speedvac Plus (Thermo Electron Corporation, Waltham, MA, USA). The methylated peptide was mixed with the metal complexes in each experiment without any further purification.

Mass Spectrometry

All mass spectrometry experiments were conducted using a quadrupole ion trap mass spectrometer (Finnigan LCQ, ThermoFinnigan, San Jose, CA, USA). Samples typically consisted of 600 μM Cu(II) complex and

50 μM peptide in a water/MeOH (50:50) solution. These samples were infused continuously at a typical rate of 5 μL/min into the pneumatically assisted electrospray probe, using air as the nebulizer gas. CID

spectra of $[Cu^{II}(L)M]^{\bullet 2+}$ complexes [where L = dien or 9-aneN$_3$; M = glycylglycylhistidine (GlyGlyHis), histidine (His), or methylated histidine (His+OMe)] were acquired using He as the collision gas. The injection and
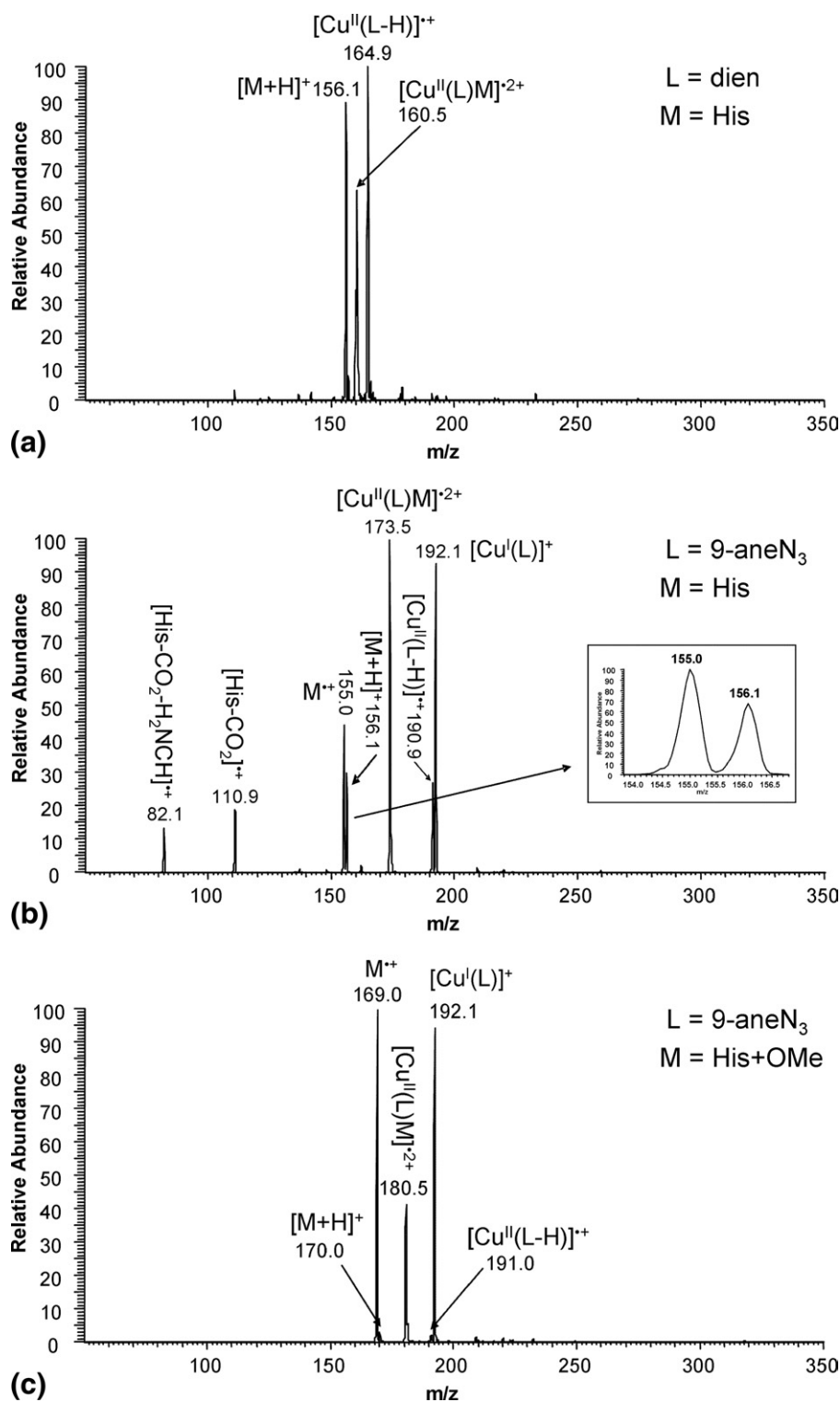
Figure 1. CID spectra (with unimass resolution) of $[Cu^{II}(L)His]^{\bullet 2+}$ complexes: (**a**) L = dien; M = His; (**b**) L = 9-aneN$_3$; M = His; (**c**) L = 9-aneN$_3$; M = His + OMe. The amplitudes of the resonance excitation RF voltage were 0.49, 0.45, and 0.41 eV, respectively. Inset to (**b**): Zoom scan spectrum of His$^{\bullet +}$ and [His + H]$^+$.

activation times for CID in the ion trap were 200 and 30 ms, respectively; the amplitude of the excitation was optimized for each experiment.

Computational Methods

All DFT calculations were conducted using the GAUSSIAN03 software package [28]. DFT was used to determine the geometries, energetics, Mulliken distribution, and natural population analysis (NPA) of the charge and spin density. The B3LYP functional—with Becke's three-parameter hybrid exchange (B3) [29] and the correlation functional of Lee, Yang, and Parr (LYP) [30]—was used with a moderate double-zeta 6-31+G(d) basis set [31]; for some structures, single-point energy and full optimization calculations at the B3LYP/6-311++G(d,p) level of theory were performed to consider the basis set effect. Harmonic vibrational frequen-

cies of all of the structures were calculated at the B3LYP/6-31+G(d) level to confirm local minima with all real frequencies and transition-state structures having one imaginary frequency. The local minima of each transition structure were verified using the intrinsic reaction coordinate (IRC) method. Relative enthalpies at 0 K ($\Delta H°_0$) were calculated from electronic energies and zero-point energies (ZPVE).

The bonding character and charge distribution for some stationary points were determined using quantum theory of atoms in molecules (QTAIM) [32, 33], which is well suited to studying the properties of weak bonds. The topological properties of the electron density distribution of each molecule were determined based on the gradient vector field of the electron density $\rho(r)$ and on the Laplacian of the electron density $\nabla^2\rho(\mathbf{r})$, where $\mathbf{r}$ is the positional vector of an electron in three-dimensional space. The molecular graphs—including
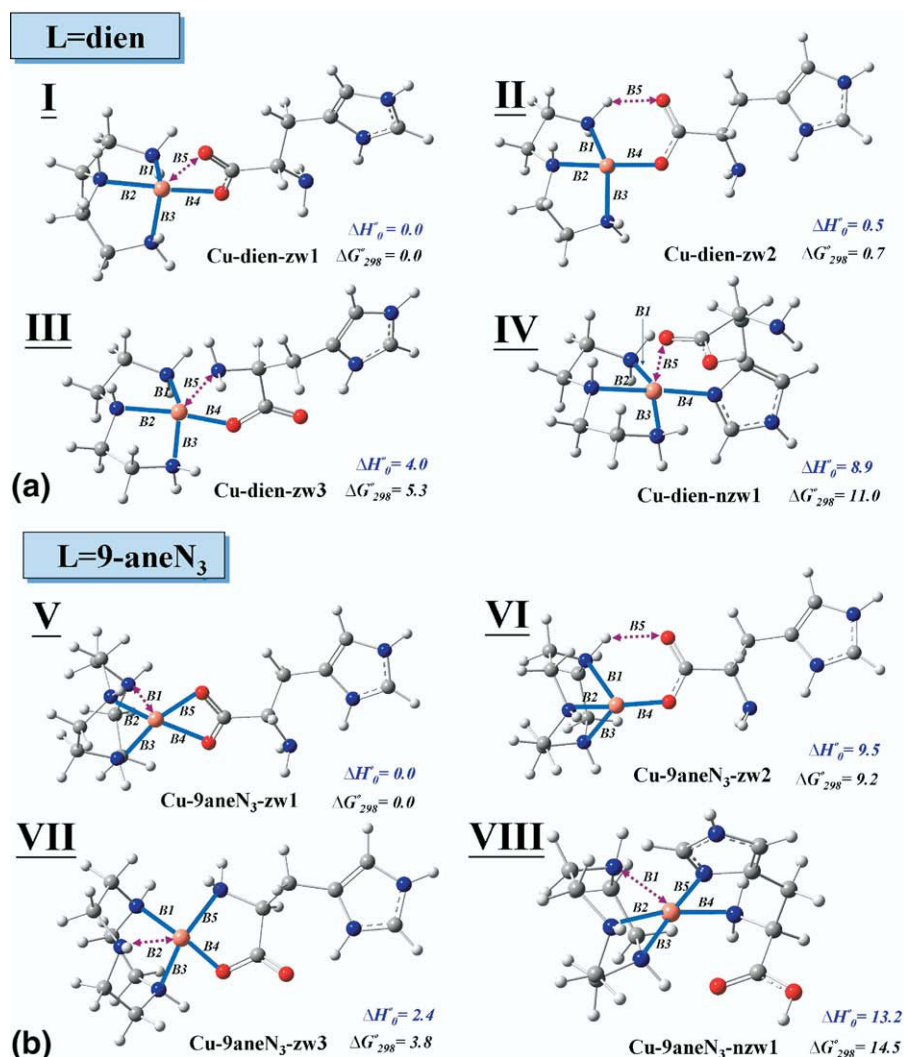
Figure 2. Selected geometries (specified in Table 2; Å) and relative enthalpies and free energies (kcal/mol) predicted for the three lowest-energy zwitterionic complexes and one lowest-energy non-zwitterionic complex of (**a**) [Cu^{II}(dien)His]$^{•2+}$ and (**b**) [Cu^{II}(9-aneN$_3$)His]$^{•2+}$ at the B3LYP/6-31+G(d) level. Blue bold bonds represent relatively strong coordination (electron density of BCP ≅ 0.0700–0.0900 au) between two atoms.

bond critical points (BCPs), ring critical points (RCPs), and cage critical points (CCPs)—and the bond paths were plotted using the AIM2000 program [34, 35]; atomic integration [36] for each atom in a molecule, based on B3LYP/6-31+G(d) wave functions, was performed using the AIMALL program [37].

Results and Discussion

To acquire a better fundamental understanding of the role of sterically constrained ligands, we investigated the structures and dissociation energetics of prototypical $[Cu^{II}(dien)His]^{\bullet 2+}$ and $[Cu^{II}(9\text{-aneN}_3)His]^{\bullet 2+}$ ions using low-energy CID experiments and DFT calculations. We examined $[Cu^{II}(dien)His]^{\bullet 2+}$ and $[Cu^{II}(9\text{-aneN}_3)His]^{\bullet 2+}$ systems partly because their CID spectra (Figure 1a and b) bear a strong resemblance to those of $[Cu^{II}(dien)GlyGlyHis]^{\bullet 2+}$ and $[Cu^{II}(9\text{-aneN}_3)GlyGlyHis]^{\bullet 2+}$ [16] (see Figure 1S in the supplementary material, which can be found in the electronic version of this article) and partly because the gas-phase structures of both radical cationic and protonated histidine have been examined theoretically in previous studies [38, 39, 43]. The dissociations of both $[Cu^{II}(dien)His]^{\bullet 2+}$ and $[Cu^{II}(9\text{-aneN}_3)His]^{\bullet 2+}$ proceed through PT reactions to produce protonated histidine $[His + H]^+$; importantly, the latter system facilitates the generation of two isomeric histidine radical cations having non-zwitterionic forms ($[His_{NZW}]^{\bullet +}$) at m/z 155 and zwitterionic form ($[His_{ZW}]^{\bullet +}$, also known as the "type 2 histidine radical cations" or distonic ions) [39]. $[His_{ZW}]^{\bullet +}$ undergoes

spontaneously consecutive fragmentations to form the ions $[His - CO_2]^{\bullet +}$ at m/z 111 and $[His - CO_2 - H_2NCH]^{\bullet +}$ at m/z 82 [39]. Previous studies—and the results presented in Figure 1b—provided evidence for the facile dissociation of the transient and nonisolable $[His_{ZW}]^{\bullet +}$ [39].

We established the identity of the non-zwitterionic $[His_{NZW}]^{\bullet +}$ radical cation formed from $[Cu^{II}(9\text{-aneN}_3)His]^{\bullet 2+}$ through comparison of the CID spectra of $[His_{NZW}]^{\bullet +}$ and $[His+OMe]^{\bullet +}$ obtained from $[Cu^{II}(9\text{-aneN}_3)His]^{\bullet 2+}$ and $[Cu^{II}(9\text{-aneN}_3)(His + OMe)]^{\bullet 2+}$, respectively, where His + OMe, the histidine methyl ester, can exist only in its non-zwitterionic (canonical) form. The dissociation of $[Cu^{II}(9\text{-aneN}_3)(His + OMe)]^{\bullet 2+}$ produced intact $[His + OMe]^{\bullet +}$ solely; i.e., the secondary product ions of the metastable zwitterionic radical were absent in Figure 1c. The CID spectra of the stable and intact $[His_{NZW}]^{\bullet +}$ and $[His + OMe]^{\bullet +}$ radical cations are almost identical, generating the fragment ions $[b_1 - H]^{\bullet +}$ and $[a_1 - H]^{\bullet +}$ (see Supplemental Figure 2S). These spectra provide additional experimental evidence for the non-zwitterionic identity of the isolable $[His_{NZW}]^{\bullet +}$.

Structures of $[Cu^{II}(L)His]^{\bullet 2+}$ Complexes

We systematically explored the structures and relative energies of the precursor complexes and their related major product ions through DFT calculations. Figure 2a and b display the four lowest-energy structures of the $[Cu^{II}(dien)His]^{\bullet 2+}$ and $[Cu^{II}(9\text{-aneN}_3)His]^{\bullet 2+}$ com-

Table 1. Relative total electronic energies (ΔE_{total}, kcal/mol) and selected bond properties predicted for $[Cu^{II}(L)His]^{\bullet 2+}$ complexes

	$\Delta E_{total}{}^a$	$\Delta E_{total}{}^b$	$\Delta E_{total}{}^c$	B1	B2	B3	B4	B5
Cu-dien-zw1	0.0	0.0	0.0	2.07^d	2.05	2.06	1.98	2.37
				2.08^e	*2.06*	*2.07*	*1.99*	*2.38*
				0.0810^f	0.0856	0.0898	0.0868	0.0367
Cu-dien-zw2	0.4	−0.3	−0.3	2.03	2.07	2.06	1.92	1.99
				2.03	*2.07*	*2.06*	*1.93*	*1.99*
				0.0910	0.0836	0.0840	0.0984	0.0257
Cu-dien-zw3	3.8	3.4	3.4	2.09	2.07	2.09	1.92	2.38
				2.10	*2.08*	*2.09*	*1.93*	*2.37*
				0.0776	0.0816	0.0784	0.0963	0.0414
Cu-dien-nzw1	8.9	6.7	6.7	2.08	2.05	2.09	2.04	2.28
				2.09	*2.05*	*2.10*	*2.04*	*2.28*
				0.0800	0.0880	0.0791	0.0826	0.0400
Cu-9aneN₃-zw1	0.0	0.0	0.0	2.04	2.03	2.06	2.32	2.02
				2.05	*2.05*	*2.06*	*2.32*	*2.03*
				0.0481	0.0915	0.0892	0.0727	0.0782
Cu-9aneN₃-zw2	9.6	9.1	9.0	2.09	1.99	2.19	1.86	2.11
				2.10	*2.00*	*2.19*	*1.87*	*2.14*
				0.0798	0.0975	0.0648	0.1131	0.0199
Cu-9aneN₃-zw3	1.7	1.3	1.2	2.07	2.36	2.04	1.93	2.11
				2.07	*2.35*	*2.05*	*1.94*	*2.12*
				0.0824	0.0450	0.0886	0.0958	0.0728
Cu-9aneN₃-nzw1	12.5	10.2	10.4	2.43	2.07	2.10	2.11	2.07
				2.42	*2.08*	*2.10*	*2.12*	*2.07*
				0.0386	0.0819	0.0776	0.0730	0.0770

$^a\Delta E_{total}$ of structures geometry*; $^b\Delta E_{total}$ of structures geometry#; $^c\Delta E_{total}$ of single-point energies*#; ^{d}bond lengths (Å) of structures*; ^{e}bond lengths (Å)#; ^{f}electron density (au) of BCP calculated by AIM2000. *B3LYP/6-31+G(d). #B3LYP/6-311++G(d,p).

Table 2. Enthalpies (ΔH°_0, kcal/mol) and free energies (ΔG°_{298}, kcal/mol) predicted at the B3LYP/6-31+G(d) level for the formation of **Cu-L-zw1**, **Cu-L-zw2**, **Cu-L-zw1 zw3**, and **Cu-L-nzw1**[a]

| Reaction	Ligand (L) type	ΔH°_0	ΔG°_{298}
$[Cu^{II}(L)]^{\bullet 2+}$ + $[His_{zw1}]$ →	dien	−102.9	−91.8
Cu-L-zw1	9-aneN$_3$	−119.2	−107.2
$[Cu^{II}(L)]^{\bullet 2+}$ + $[His_{zw2}]$ →	dien	−102.4	−91.1
Cu-L-zw2	9-aneN$_3$	−109.6	−98.0
$[Cu^{II}(L)]^{\bullet 2+}$ + $[His_{zw3}]$ →	dien	−90.1	−77.5
Cu-L-zw3	9-aneN$_3$	−107.9	−94.5
$[Cu^{II}(L)]^{\bullet 2+}$ + $[His_{nzw1}]$ →	dien	−83.7	−70.2
Cu-L-nzw1	9-aneN$_3$	−102.6	−88.5

[a]The structures of His are at local minima, optimized from the geometries of the His fragment in the corresponding $[Cu^{II}(L)His]^{\bullet 2+}$ complex.

plexes. For each system, three of the structures possess zwitterionic forms with a proton on the imidazole nitrogen atom (**I–III** and **V–VII**) and the fourth structure possesses a lowest energy structure of non-zwitterionic form (**IV** and **VIII**).

In Figure 2, the bold blue bonds indicate relatively strong coordination, with electron density of the BCPs of roughly 0.0700–0.0900 au (see Table 1), between the nitrogen or oxygen atoms and the Cu(II) center. The three nitrogen atoms of the dien ligand all coordinate strongly to the Cu(II) ion, leaving only one unoccupied site for binding to His. In contrast, steric encumbrance means that only two of the nitrogen atoms of the macrocyclic 9-aneN$_3$ could coordinate strongly to the

Cu(II) ion, thereby leaving two free coordination sites for relatively strong His chelation [19, 40]; these structures are consistent with the higher binding energies of $[Cu^{II}(9\text{-}aneN_3)His]^{\bullet 2+}$ (see Table 2). For example, the binding energies of **Cu-9aneN$_3$-zw1** and **Cu-9aneN$_3$-zw3** are 16.3 and 17.8 kcal/mol higher than those of **Cu-dien-zw1** and **Cu-dien-zw3**, respectively. The different binding modes and forms of His (zwitterionic or non-zwitterionic structures) within the Cu(II) complexes in the gas phase resulted in pronounced differences in reactivity, as revealed in recent studies [38, 39] as well as in Supplemental Figure 2S.

$[Cu^{II}(dien)His]^{\bullet 2+}$ **(I–IV)**. Table 1 reveals that the relative energy differences obtained using the two sets of basis sets, 6-31+G(d) and 6-311++G(d,p), were less than 2.2 kcal/mol, and those for the Cu—N and Cu—O bond lengths differed by less than 0.03 Å. Because there is no obvious basis set effect, our following discussions refer only to the structures obtained through B3LYP/6-31+G(d) calculations, except where noted. The Cu(II) centers in **I**, **III**, and **IV** possess distorted square pyramidal and trigonal bipyramidal geometries. The tridentate auxiliary dien ligand is coordinated meridianally to the Cu(II) ion and the other two coordination sites are occupied by the His unit [19, 40], which possesses either a zwitterionic or non-zwitterionic structure. **Cu-dien-zw2** is stabilized by a six-membered ring containing a weak N—H···O=C hydrogen bond (bond length: 1.99 Å; purple double-headed arrow in Figure 2a-II) between the amino hydrogen atom of dien and the other car-
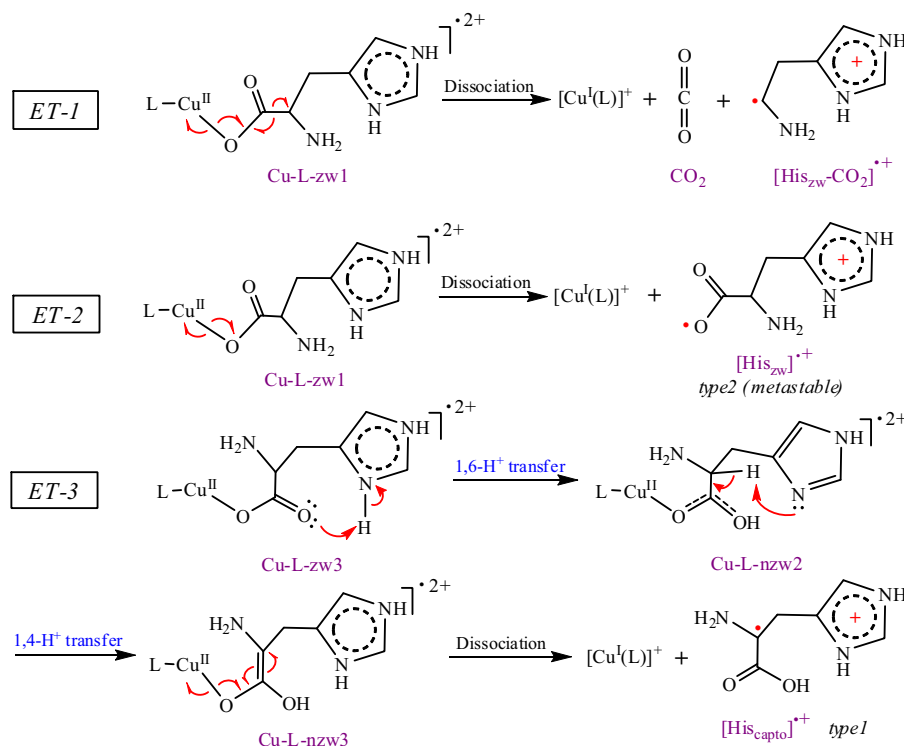

Scheme 1. ET reactions of $[Cu^{II}(L)His]^{\bullet 2+}$ complexes calculated at the B3LYP/6-31+G(d) level.

boxyl oxygen atom of His, making the **zw1** and **zw2** structures almost degenerate in energy. Therefore, we would expect **zw1** and **zw2** to coexist in the reactant. **Cu-dien-zw3** is mono-coordinated by one carboxyl oxygen atom with an additional weaker interaction (electron density of BCP: 0.0414 au) with the N-terminal amino group of the His unit; this structure is higher in energy than the **zw1** form by 4.0 kcal/mol. Thus, we cannot rule out the possibility of **zw1** and **zw3** coexisting during the initial stages of the reaction because of the limited accuracy (~2–3 kcal/mol) of the DFT calculations [41, 42]. The non-zwitterionic **Cu-dien-nzw1** contains a salt-bridge structure for the His unit in the complex, with a Cu(II)—N1$_{imidazole}$ bond and an additional long-range O—Cu interaction with the carboxyl oxygen atom. This isomer is 8.9 kcal/mol higher in energy than the **Cu-dien-zw1** structure.

$[Cu^{II}(9\text{-aneN}_3)His]^{\bullet 2+}$ (V–VIII).

Figure 2b presents optimized structures of the four lowest-energy isomers of the $[Cu^{II}(9\text{-aneN}_3)His]^{\bullet 2+}$ complex. The lowest-energy complex **Cu-9aneN$_3$-zw1** on the PES features the Cu(II)

center occupied by the two C-terminal carboxyl oxygen atoms of the zwitterionic His unit; one of the N$_{9\text{-aneN3}}$—Cu^{II} bonds is notably longer than those of the other two. The electron densities at the BCPs of B1, B2, and B3 are 0.0481, 0.0915, and 0.0892 au, respectively. The **Cu-9aneN$_3$-zw2** structure features a substantially different binding mode: only one carboxyl oxygen atom interacts with a lobe of the d$_{xy}$ orbital of Cu(II). The other oxygen atom is stabilized through hydrogen bonding with a secondary amino group of 9-aneN$_3$. This structure is the least energetically favorable among the zwitterionic structures: the **Cu-9aneN$_3$-zw2** complex is higher in enthalpy than the **Cu-9aneN$_3$-zw1** and **Cu-9aneN$_3$-zw3** structures by 9.5 and 7.1 kcal/mol, respectively; nevertheless, it is still 3.7 kcal/mol lower in enthalpy than the **Cu-9aneN$_3$-nzw1** isomer, the lowest-energy non-zwitterionic His complex. The relative energy difference between **Cu-9aneN$_3$-zw1** and **Cu-9aneN$_3$-zw3** is about 2.4 kcal/mol. Thus, we predict that the $[Cu^{II}(9\text{-aneN}_3)His]^{\bullet 2+}$ radical cation can adopt both **Cu-9aneN$_3$-zw1** and **Cu-9aneN$_3$-zw3** forms. Siu's recent work—theoretical calculations at the UB3LYP/6-
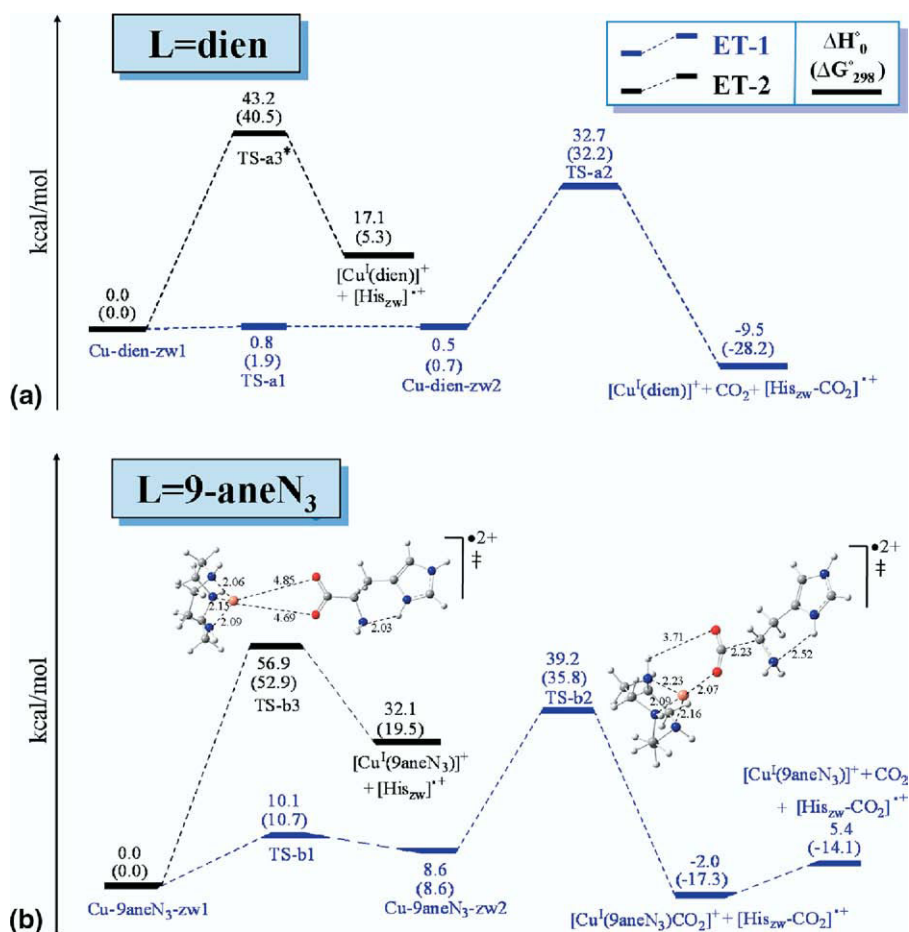
Figure 3. Reaction profiles predicted for the ET dissociations [*ET-1* (blue); *ET-2* (black)] of the (**a**) **Cu-dien-zw1** and (**b**) **Cu-9aneN$_3$-zw1** complexes at the B3LYP/6-31+G(d) level. The upper and lower (in parenthesis) numbers are relative enthalpies and free energies (kcal/mol), respectively. The asterisk on **TS-a3** indicates that this structure has a redundant imaginary frequency (-9.048 cm^{-1}). A potential energy scan along the Cu···O distance from **Cu-dien-zw1** has been acquired (Figure 3S) [49].

31++G(d,p) level and experimental measurements of the infrared multiple photon dissociation (IRMPD) spectrum of $His^{\bullet+}$—have also revealed that the observable $His^{\bullet+}$ from the dissociation of $[Cu^{II}(terpy)His]^{\bullet 2+}$ possesses the captodative structure. In contrast, the alternative structures of histidine on $[Cu^{II}(terpy)His]^{\bullet+}$ complexes involves both canonical (80%) and zwitterionic (20%) forms [43]. Our finding of more localized charge on the copper center of $[Cu^{II}(dien)His]^{\bullet+}$ complexes might be ascribable to favorable zwitterionic His binding, stemming from the weaker interaction between the auxiliary dien ligand and the copper(II) center in $[Cu^{II}(dien)His]^{\bullet+}$ [39].

Energetics of Complex Dissociation

ET reactions. Previous experimental and theoretical results have revealed two types of His radical cations: (1) an isolable His radical cation ($[\mathbf{His_{capto}}]^{\bullet+}$, also known as "type 1 $His^{\bullet+}$") [39], possessing captodative character with an α-carbon-centered radical featuring adjacent π-donor (NH_2) and π-acceptor (COOH) units [44–48], which is stable on the timescale of our mass spectrometric experiments; and (2) a transitory zwitterionic His radical cation that is too unstable to be detected directly; it is detected instead through the facile formation of $[\mathbf{His_{zw}} - \mathbf{CO_2}]^{\bullet+}$. We examined three dissociative electron-transfer pathways for $[Cu^{II}(L)(His)]^{\bullet 2+}$: (1) the formation of the transitory zwitterionic His radical cation to produce $[\mathbf{His_{zw}} - \mathbf{CO_2}]^{\bullet+}$ (*ET-1* in Scheme 1), (2) the direct formation of the intact zwitterionic His radical cation $[\mathbf{His_{zw}}]^{\bullet+}$ with substantial higher energy barriers (*ET-2*), and (3) the formation of the intact captodative His radical cation $[\mathbf{His_{capto}}]^{\bullet+}$ through two consecutive PT steps (*ET-3*). Figures 3 and 5 display the potential energy surfaces for $[Cu^{II}(L)(His)]^{\bullet 2+}$ (L = dien or 9-aneN_3).

In *ET-1*, the isomerization of **Cu-L-zw1** to **Cu-L-zw2** has an energy barrier of 1.9 (10.7) kcal/mol in free-energy (hereafter) via the transition-state **TS-a1** (**TS-b1**) by breaking one of the two Cu(II)—O bonds when L is dien (9-aneN_3); these values are consistent with the stronger binding of Cu(II) and His in the presence of sterically encumbered 9-aneN_3. The facile cleavage of the C_α—CO_2 and Cu(II)—O bonds of **Cu-L-zw2** via **TS-a2** and **TS-b2**, respectively, is the rate-determining step in *ET-1*, with barriers of 32.2 and 35.8 kcal/mol for the dien and 9-aneN_3 ligands, respectively.

The energy barriers of *ET-2* leading to intact $[\mathbf{His_{zw}}]^{\bullet+}$—40.5 and 52.9 kcal/mol for dien and 9-aneN_3 ligands, respectively—are the highest among the three pathways. The AIM, NPA, and Mulliken charge distributions of the transition states in *ET-1* and *ET-2* for the $[Cu^{II}(9\text{-ane}N_3)His]^{\bullet 2+}$ complexes (Figure 4) reveal that a salt bridge (—CO_2—) with negative charge exists between the two positively charged parts in **TS-b2**, stabilizing and greatly reducing columbic repulsion in the system. The topological analysis using AIM in Figure 4 indicated that even the fairly long bond
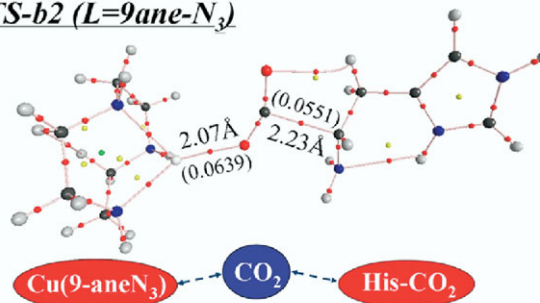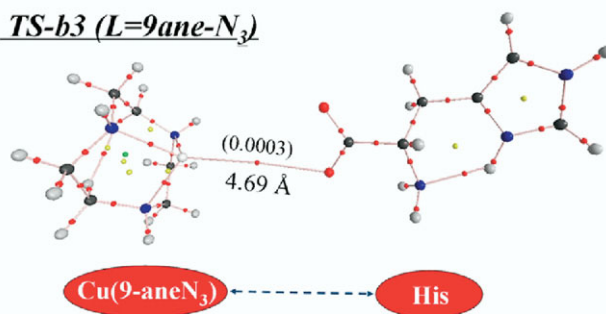
Figure 4. AIM, NPA, and Mulliken charge distributions for **TS-b2** and **TS-b3**, calculated using the AIMALL and Gaussian 03 programs. The bond paths were plotted using the AIM2000 program. BCPs are indicated with red dots with electron density values (au).

length (4.69 Å) preserves the very weak interaction between the two portions in **TS-b3**; the existence of this long bond is further evidenced by an electron density of 0.0003 au at this bond critical point. The high energy of **TS-b3** can be ascribed to coulombic repulsion between product ions having the same positive charge. The components of the solvated trimer **Cu(9-aneN_3)⋯CO_2⋯[His − CO_2]** in **TS-b2** are separated by 2.07 and 2.23 Å, respectively (Figure 3); these values are typical for transition-state structures. The bond order of the structure is also characterized by electron densities of 0.0639 and 0.0553 au at the BCPs, implying their long-range order.

Figure 5 displays the potential energy surface for the origin of $[\mathbf{His_{capto}}]^{\bullet+}$. Converting from the zwitterionic **Cu-L-zw3** to the non-zwitterionic **Cu-L-nzw2** complex involves a 1,6 proton shift from the N_π atom of the imidazole ring to the uncoordinated carboxyl oxygen atom. **Cu-dien-nzw2** and **Cu-9aneN_3-nzw2** are 21.4 and 22.0 kcal/mol higher in energy than **Cu-dien-zw3** and **Cu-9aneN_3-zw3**, respectively. The barriers of these tautomerization reactions are 37.4 and 37.5 kcal/mol, respectively (relative to **Cu-L-zw1**, hereafter). A 1,4 pro-
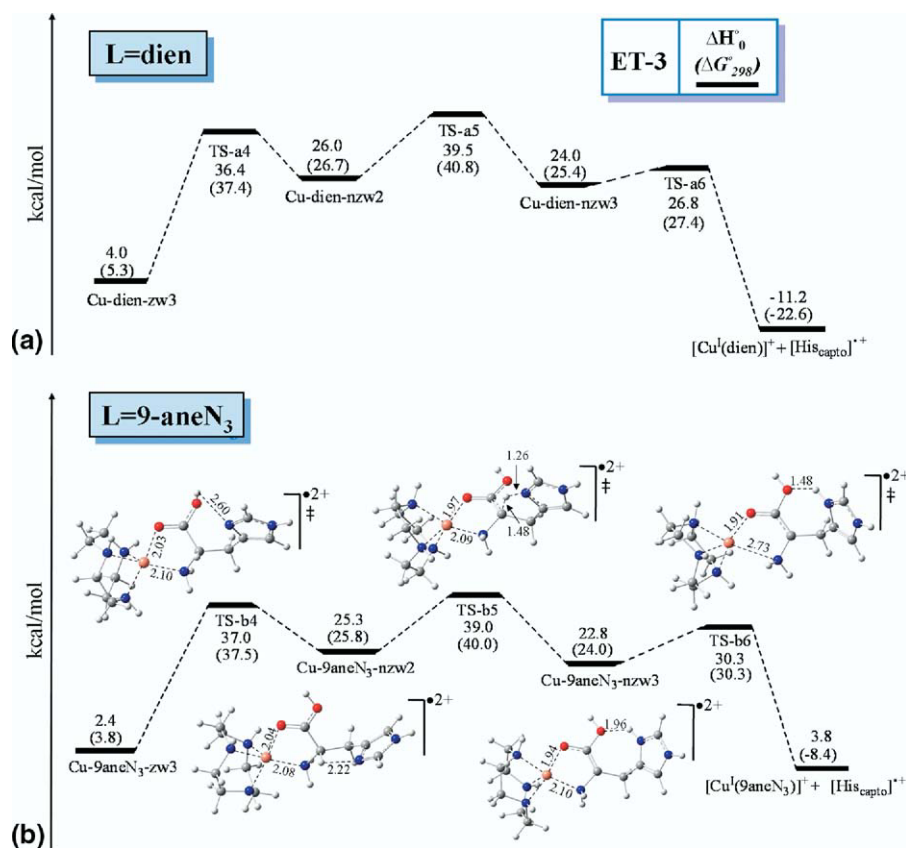
Figure 5. Reaction profiles predicted for the *ET-3* dissociations of the (**a**) **Cu-dien-zw3** and (**b**) **Cu-9aneN₃-zw3** complexes at the B3LYP/6-31+G(d) level. The upper and lower (in parenthesis) numbers are relative enthalpies and free energies (kcal/mol), respectively.

ton transfer of the hydrogen atom on the α-carbon atom to the imidazole N_π atom via **TS-a5** (L = dien) and **TS-b5** (L = 9-aneN₃) produces the **Cu-L-nzw3** complexes; the energy barriers of these processes are 14.1 and 14.2 kcal/mol, respectively. The ET reactions of **Cu-L-nzw3** (*ET-3*) proceed spontaneously with energy barriers of 2.0 (**TS-a6**; L = dien) and 6.3 kcal/mol (**TS-b6**; L = 9-aneN₃) after overcoming the second barrier attributed to the unstable intermediate **Cu-L-nzw3**.

We used NPA to keep track of the charge and spin density in each transition-state; Table 3 displays the transition states of ET-1, ET-2, and ET-3 and their associated minima before ET reactions. We observed a reduction in the amount of charge for all of the Cu(L) species upon proceeding from the Cu(II) complex to the transition-state complex, in accordance with the expected change in oxidation state from Cu(II) to Cu(I). The spin density provides further evidence for this change. The increases of spin density values for all of the His fragments upon proceeding from the minima to the transition-state are consisted with the formation of the His radical cation.

PT reactions. PT of $[Cu^{II}(dien)His]^{•2+}$ to the carboxyl oxygen atom can occur through three pathways

(Figure 6a): (**PT-CH₂**) directly from the methylene hydrogen atom via transition structure **TS-a11**; the barrier against this reaction has the highest energy on the PES at 41.0 kcal/mol (relative to **Cu-dien-zw1** hereafter); (**PT-NH₂**) from the NH₂ group through three consecutive tautomerizations via transition structures

Table 3. Natural population analysis at the B3LYP/6-31+G(d) level of transition states of the ET step for **ET-1**, **ET-2**, and **ET-3** and the minima prior to transfer[a]

	Charge		Spin density	
	Cu(L)	His-fragment	Cu(L)	His-fragment
Cu-dien-zw2	1.762	0.238	0.884	0.116
TS-a2	1.055	0.945	0.091	0.909
Cu-9aneN₃-zw2	1.738	0.262	0.878	0.122
TS-b2	1.038	0.962	0.094	0.906
Cu-dien-zw1	1.756	0.244	0.878	0.122
TS-a3	1.174	0.826	0.175	0.825
Cu-9aneN₃-zw1	1.688	0.312	0.830	0.170
TS-b3	1.141	0.859	0.142	0.858
Cu-dien-nzw3	1.754	0.246	0.881	0.119
TS-a6	1.664	0.336	0.758	0.242
Cu-9aneN₃-nzw3	1.668	0.332	0.816	0.184
TS-b6	1.393	0.607	0.493	0.507

[a]The sums of the charge and spin density of the system are 2.000 and 1.000, respectively.
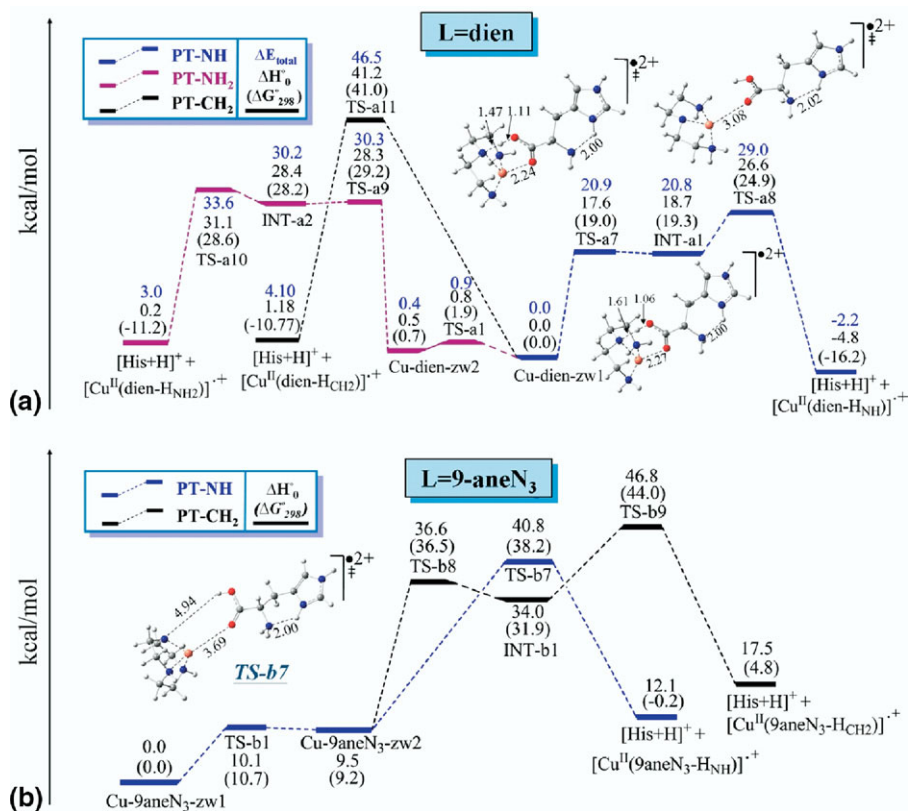
Figure 6. Reaction profiles predicted for the PT dissociations of (**a**) **Cu-dien-zw1** and (**b**) **Cu-9aneN₃-zw1** at the B3LYP/6-31+G(d) level. The upper and lower (in parenthesis) numbers are relative enthalpies and free energies (kcal/mol), respectively. The numbers in blue are relative total electronic energies (kcal/mol).

TS-a1, **TS-a9**, and **TS-a10** and intermediates **Cu-dien-zw2** and **INT-a2**; the rate-determining step for this multistep process occurs through the critical intermediate **INT-a2** with an energy barrier of 29.2 kcal/mol, with subsequent direct dissociation to yield products with energy barriers as low as 0.4 kcal/mol; or (**PT-NH**) from a secondary amino NH group via two consecutive tautomerizations proceeding through transition structures **TS-a7** and **TS-a8** and the intermediate **INT-a1**, which has a very shallow barrier relative to **TS-a7**, but a rather large one relative to **TS-a8**; the barrier against this pseudo-two-step reaction is 24.9 kcal/mol. Figure 6a presents the PES for each of the reactions. We attribute the highest energy barrier for PT involving the methylene hydrogen atom in reaction PT-CH₂ to the greater strength of the C—H bond relative to that of the N—H bond. In comparison, the difference between the barriers of reactions PT-NH₂ and PT-NH involving amino hydrogen atoms is 4.3 kcal/mol; i.e., the values are comparable. These DFT results suggest that both channels are competitive.

PT of [Cu^{II}(9-aneN₃)His]$^{\bullet2+}$ begins through the carboxyl oxygen atom approaching the NH group of 9-aneN₃ to form the critical structure of **Cu-9aneN₃-zw2** via **TS-b1**. Two subsequent competitive reaction pathways are possible (Figure 6b): (**PT-NH**), a simple intramolecular PT from the NH group to the carboxyl

oxygen atom via **TS-b7** with a relatively long distance (3.69 Å) between the carboxyl oxygen atom and the Cu(II) ion; the energy barrier of 38.2 kcal/mol is thermally favorable when considering the lower total free energies of the product ions [His + H]$^+$ and [Cu^{II}(9aneN₃ − H$_{NH}$)]$^{\bullet+}$ relative to that of **Cu-9aneN₃-zw1**; (**PT-CH₂**), two sequential interconversions that are similar to the PT reaction (PT-NH) of [Cu^{II}(dien)His]$^{\bullet2+}$ via the transition structures **TS-b8** and **TS-b9** and the intermediate **INT-b1** and subsequent intramolecular PT from the CH₂ group to the carboxyl oxygen atom, resulting in the product ions [His + H]$^+$ and [Cu^{II}(9aneN₃ − H$_{CH2}$)]$^{\bullet+}$; the rate-determining step of this two-step process is 44.0 kcal/mol.

[Cu^{II}(dien)His]$^{\bullet2+}$ and [Cu^{II}(9-aneN₃)His]$^{\bullet2+}$ complexes have quite different electronic structures and coordination geometries: the former is coordinated by one lobe of the d$_{xy}$-type orbital; the latter is doubly coordinated by two lobes of the d$_{xy}$-type orbital as a result of the relatively high binding energies of His (−91.8 and −107.2 kcal/mol, respectively; Table 2). The macrocyclic [Cu^{II}(9-aneN₃)His]$^{\bullet2+}$ complex has substantially higher intramolecular PT barriers than those of the [Cu^{II}(dien)His]$^{\bullet2+}$ complex because of the restricted binding of His for any critical rotation. In contrast, the His unit in the [Cu^{II}(dien)(His)]$^{\bullet2+}$ complex allows free translation of the carbonyl oxygen atom
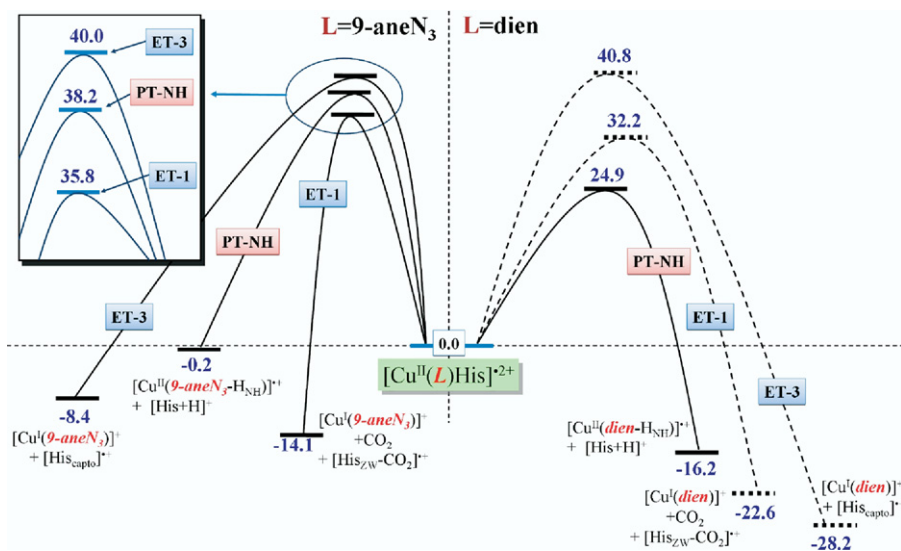
Scheme 2. Relative free energies (kcal/mol) of the competitive ET and PT reactions for the (left) $[Cu^{II}(9\text{-aneN}_3)His]^{\bullet 2+}$ and (right) $[Cu^{II}(dien)His]^{\bullet 2+}$ complexes, calculated at the B3LYP/6-31+G(d) level. The observed facile reaction pathways are indicated by the solid lines; the suppressed reaction pathways are indicated by the broken lines. Only key transition structures of competitive pathways are shown.

from Cu—O to the NH group for the subsequent PT. This feature suggests that the lower steric constraint of the auxiliary ligand in the $[Cu^{II}(dien)(His)]^{\bullet 2+}$ complex is a crucial factor facilitating PT via two consecutive tautomerizations proceeding through the transition structures **TS-a7** and **TS-a8**. In summary, the most favorable PT pathway of the $[Cu^{II}(dien)His]^{\bullet 2+}$ complex is energetically more favorable by 13.3 kcal/mol than that of the corresponding $[Cu^{II}(9\text{-aneN}_3)His]^{\bullet 2+}$ complex.

PT versus ET Dissociations

Scheme 2 summarizes the lowest reaction barriers of the ET and PT reactions for the $[Cu^{II}(L)His]^{\bullet 2+}$ complexes (L = dien or 9-aneN₃).

The most energetically favorable PT pathway corresponds to PT-NH of the auxiliary ligand of $[Cu^{II}(L)His]^{\bullet 2+}$. The barrier of $[Cu^{II}(9\text{-aneN}_3)His]^{\bullet 2+}$ for this PT-NH pathway (38.2 kcal/mol) is comparable with the barriers for the two lowest-energy degenerate ET reactions of the **ET-1** (35.8 kcal/mol) and **ET-3** (40.0 kcal/mol) pathways. The difference between reaction barriers of $[Cu^{II}(9\text{-aneN}_3)His]^{\bullet 2+}$ and $[Cu^{II}(dien)His]^{\bullet 2+}$ in **ET-1** is 3.6 kcal/mol to produce $[His_{zw} - CO_2]^{\bullet +}$; in **ET-3** it is negligible to produce the intact isolable $[His_{capto}]^{\bullet +}$. The PT-NH process of $[Cu^{II}(dien)His]^{\bullet 2+}$ is energetically more favorable than its competitive **ET-1** pathway by 7.3 kcal/mol. This result explains the exclusive formation of PT products from the complex, including protonated His and its complementary deprotonated $[Cu^{II}(dien - H)]^{\bullet +}$ ion in the CID experiment (Figure 1a). In summary, we have demonstrated, through low-energy CID experiments and DFT calculations, that the sterically

constrained $[Cu^{II}(9\text{-aneN}_3)His]^{\bullet 2+}$ complex facilitates ET to produce the His radical cation and its fragment ions by moderating the competitive PT reaction pathways.

Conclusion

To elucidate the mechanisms of the enhanced peptide radical cation formation that arise from the macrocyclic effect of the auxiliary ligand in $[Cu^{II}(L)His]^{\bullet 2+}$ complexes, we have performed DFT calculations, at the B3LYP/6-31+G(d) level, of the major competitive reactions of the $[Cu^{II}(dien)His]^{\bullet 2+}$ complex and its cyclic analogue $[Cu^{II}(9\text{-aneN}_3)His]^{\bullet 2+}$. Both complexes have similar energy barriers for their ET pathways. In contrast, the greater steric constraint provided by the auxiliary ligand in the $[Cu^{II}(9\text{-aneN}_3)His]^{\bullet 2+}$ complex leads to inefficient PT; this effect is responsible for shifting the dissociation pathway from PT toward ET, consistent with our experimental observations.

Acknowledgments

Appendix A
Supplementary Material

Supplementary material associated with this article may be found in the online version at doi:10.1016/ j.jasms.2009.01.007.

References

1. Holm, R. H.; Kennepohl, P.; Solomon, E. I. Structural and Functional Aspects of Metal Sites in Biology. *Chem. Rev.* **1996**, *96*, 2239–2314.
2. Opazo, C.; Huang, X. D.; Cherny, R. A.; Moir, R. D.; Roher, A. E.; White, A. R.; Cappai, R.; Masters, C. L.; Tanzi, R. E.; Inestrosa, N. C.; Bush, A. I. Metalloenzyme-like Activity of Alzheimer's Disease Beta-Amyloid: Cu-Dependent Catalytic Conversion of Dopamine, Cholesterol, and Biological Reducing Agents to Neurotoxic H$_2$O$_2$. *J. Biol. Chem.* **2002**, *277*, 40302–40308.
3. Huang, X. D.; Cuajungco, M. P.; Atwood, C. S.; Hartshorn, M. A.; Tyndall, J. D. A.; Hanson, G. R.; Stokes, K. C.; Leopold, M.; Multhaup, G.; Goldstein, L. E.; Scarpa, R. C.; Saunders, A. J.; Lim, J.; Moir, R. D.; Glabe, C.; Bowden, E. F.; Masters, C. L.; Fairlie, D. P.; Tanzi, R. E.; Bush, A. I. Cu(II) Potentiation of Alzheimer A Beta Neurotoxicity: Correlation with Cell-Free Hydrogen Peroxide Production and Metal Reduction. *J. Biol. Chem.* **1999**, *274*, 37111–37116.
4. Millhauser, G. L. Copper Binding in the Prion Protein. *Acc. Chem. Res.* **2004**, *37*, 79–85.
5. Lehmann, S. Metal Ions and Prion Diseases. *Curr. Opin. Chem. Biol.* 2002, 6, 187–192.
6. Stubbe, J.; van der Donk, W. A. Protein Radicals in Enzyme Catalysis. *Chem. Rev.* **1998**, *98*, 705–762.
7. Chu, I. K.; Rodriquez, C. F.; Lau, T. C.; Hopkinson, A. C.; Siu, K. W. M. Molecular Radical Cations of Oligopeptides. *J. Phys. Chem. B* **2000**, *104*, 3393–3397.
8. Chu, I. K.; Rodriguez, C. F.; Hopkinson, A. C.; Siu, K. W. M. Formation of Molecular Radical Cations of Enkephalin Derivatives via Collision-Induced Dissociation of Electrospray-Generated Copper (II) Complex Ions of Amines and Peptides. *J. Am. Soc. Mass Spectrom.* **2001**, *12*, 1114–1119.
9. Bagheri-Majdi, E.; Ke, Y. Y.; Orlova, G.; Chu, I. K.; Hopkinson, A. C.; Siu, K. W. M. Copper-Mediated Peptide Radical Ions in the Gas Phase. *J. Phys. Chem. B* **2004**, *108*, 11170–11181.
10. Wee, S.; O'Hair, R. A. J.; McFadyen, W. D. Side-Chain Radical Losses from Radical Cations Allows Distinction of Leucine and Isoleucine Residues in the Isomeric Peptides Gly-XXX-Arg. *Rapid Commun. Mass Spectrom.* **2002**, *16*, 884–890.
11. Wee, S.; O'Hair, R. A. J.; McFadyen, W. D. Comparing the Gas-Phase Fragmentation Reactions of Protonated and Radical Cations of the Tripeptides GXR. *Int. J. Mass Spectrom.* **2004**, *234*, 101–122.
12. Barlow, C. K.; Wee, S.; McFadyen, W. D.; O'Hair, R. A. J. Designing Copper(II) Ternary Complexes to Generate Radical Cations of Peptides in the Gas Phase: Role of the Auxiliary Ligand. *Dalton Trans.* **2004**, 3199–3204.
13. Barlow, C. K.; McFadyen, W. D.; O'Hair, R. A. J. Formation of Cationic Peptide Radicals by Gas-Phase Redox Reactions with Trivalent Chromium, Manganese, Iron, and Cobalt Complexes. *J. Am. Chem. Soc.* **2005**, *127*, 6109–6115.
14. Chu, I. K.; Siu, S. O.; Lam, C. N. W.; Chan, J. C. Y.; Rodriquez, C. F. Formation of Molecular Radical Cations of Aliphatic Tripeptides from Their Complexes with Cu-II(12-crown-4). *Rapid Commun. Mass Spectrom.* **2004**, *18*, 1798–1802.
15. Chu, I. K.; Lam, C. N. W.; Siu, S. O. Facile Generation of Tripeptide Radical Cations In Vacuo via Intramolecular Electron Transfer in Cu-II Tripeptide Complexes Containing Sterically Encumbered Terpyridine Ligands. *J. Am. Soc. Mass Spectrom.* **2005**, *16*, 763–771.
16. Lam, C. N. W.; Siu, S. O.; Orlova, G.; Chu, I. K. Macrocyclic Effect of Auxiliary Ligand on the Gas-Phase Dissociation of Ternary Copper(II)-GGX Complexes. *Rapid Commun. Mass Spectrom.* **2006**, *20*, 790–796.
17. Lam, C. N. W.; Ruan, E. D. L.; Ma, C. Y.; Chu, I. K. Non-Zwitterionic Structures of Aliphatic-only Peptides Mediated the Formation and Dissociation of Gas Phase Radical Cations. *J. Mass Spectrom.* **2006**, *41*, 931–938.
18. Chu, I. K.; Zhao, J.; Xu, M.; Siu, S. O.; Hopkinson, A. C.; Siu, K. W. M. Are the Radical Centers in Peptide Radical Cations Mobile? The Generation, Tautomerism, and Dissociation of Isomeric Alpha-Carbon-Centered Triglycine Radical Cations in the Gas Phase. *J. Am. Chem. Soc.* **2008**, *130*, 7862–7872.
19. Gatlin, C. L.; Tureček, F.; Vaisar, T. Copper(II) Amino Acid Complexes in the Gas Phase. *J. Am. Chem. Soc.* **1995**, *117*, 3637–3638.
20. Seymour, J. L.; Tureček, F. Structure, Energetics and Reactivity of Ternary Complexes of Amino Acids with Cu(II) and 2,2'-Bipyridine by Density Functional Theory. A Combination of Radical-Induced and Spin-Remote Fragmentations. *J. Mass Spectrom.* **2002**, *37*, 533–540.
21. Chu, I. K.; Lau, T. C.; Siu, K. W. M. Intraionic, Interligand Proton Transfer in Collision-Activated Macrocyclic Complex Ions of Nickel and Copper. *J. Mass Spectrom.* **1998**, *33*, 811–818.
22. Schroder, D.; Schwarz, H.; Wu, J. L.; Wesdemiotis, C. Long-lived Dications of Cu(H$_2$O)$^{2+}$ and Cu(NH$_3$)$^{2+}$ Do Exist! *Chem. Phys. Lett.* **2001**, *343*, 258–264.
23. Gatlin, C. L.; Rao, R. D.; Tureček, F.; Vaisar, T. Carboxylate and Amine Terminus Directed Fragmentations in Gaseous Dipeptide Complexes with Copper(II) and Diimine Ligands Formed by Electrospray. *Anal. Chem.* **1996**, *68*, 263–270.
24. Vaisar, T.; Gatlin, C. L.; Rao, R. D.; Seymour, J. L.; Tureček, F. Sequence Information, Distinction and Quantitation of C-Terminal Leucine and Isoleucine in Ternary Complexes of Tripeptides with Cu(II) and 2,2'-Bipyridine. *J. Mass Spectrom.* **2001**, *36*, 306–316.
25. Peschke, M.; Blades, A. T.; Kebarle, P. Binding Energies for Doubly-Charged Ions M^{2+} = Mg^{2+}, Ca^{2+} and Zn^{2+} with the Ligands L = H$_2$O, Acetone and N-Methylacetamide in Complexes ML$_n$$^{2+}$ for n = 1 to 7 from Gas Phase Equilibria Determinations and Theoretical Calculations. *J. Am. Chem. Soc.* **2000**, *122*, 10440–10449.
26. Armentrout, P. B. Cation-Ether Complexes in the Gas Phase: Thermodynamic Insight into Molecular Recognition. *Int. J. Mass Spectrom.* **1999**, *193*, 227–240.
27. More, M. B.; Ray, D.; Armentrout, P. B. Intrinsic Affinities of Alkali Cations for 15-crown-5 and 18-crown-6: Bond Dissociation Energies of Gas-Phase M$^+$-crown Ether Complexes. *J. Am. Chem. Soc.* **1999**, *121*, 417–423.
28. Frisch, M. J.; Trucks, G. W.; Schlegel, H. B.; Scuseria, G. E.; Robb, M. A.; Cheeseman, J. R.; Montgomery, J. A. J.; Vreven, T.; Kudin, K. N.; Burant, J. C.; Millam, J. M.; Iyengar, S. S.; Tomasi, J.; Barone, V.; Mennucci, B.; Cossi, M.; Scalmani, G.; Rega, N.; Petersson, G. A.; Nakatsuji, H.; Hada, M.; Ehara, M.; Toyota, K.; Fukuda, R.; Hasegawa, J.; Ishida, M.; Nakajima, T.; Honda, Y.; Kitao, O.; Nakai, H.; Klene, M.; Li, X.; Knox, J. E.; Hratchian, H. P.; Cross, J. B.; Bakken, V.; Adamo, C.; Jaramillo, J.; Gomperts, R.; Stratmann, R. E.; Yazyev, O.; Austin, A. J.; Cammi, R.; Pomelli, C.; Ochterski, J. W.; Ayala, P. Y.; Morokuma, K.; Voth, G. A.; Salvador, P.; Dannenberg, J. J.; Zakrzewski, V. G.; Dapprich, S.; Daniels, A. D.; Strain, M. C.; Farkas, O.; Malick, D. K.; Rabuck, A. D.; Raghavachari, K.; Foresman, J. B.; Ortiz, J. V.; Cui, Q.; Baboul, A. G.; Clifford, S.; Cioslowski, J.; Stefanov, B. B.; Liu, G.; Liashenko, A.; Piskorz, P.; Komaromi, I.; Martin, R. L.; Fox, D. J.; Keith, T.; Al-Laham, M. A.; Peng, C. Y.; Nanayakkara, A.; Challacombe, M.; Gill, P. M. W.; Johnson, B.; Chen, W.; Wong, M. W.; Gonzalez, C.; Pople, J. A.; Gaussian 03, Revision C. 02 ed.; Gaussian, Inc.: Wallingford, CT, 2004.
29. Becke, A. D. Density-Functional Thermochemistry. III. The Role of Exact Exchange. *Chem. Phys.* **1993**, *98*, 5648–5652.
30. Lee, C. T.; Yang, W.; Parr, R. G. Development of the Colle–Salvetti Correlation-Energy Formula into a Functional of the Electron-Density. *Phys. Rev. B* **1988**, *37*, 785–789.
31. Hehre, W. J.; Ditchfie, R.; Pople, J. A. Self-Consistent Molecular-Orbital Methods. XII. Further Extensions of Gaussian-Type Basis Sets for Use in Molecular-Orbital Studies of Organic-Molecules. *J. Chem. Phys.* **1972**, *56*, 2257–2261.
32. Bader, R. F. W. *Atoms in Molecules: A Quantum Theory;* Oxford University Press: Oxford, UK, 1990.
33. Bader, R. F. W. A Quantum-Theory of Molecular-Structure and Its Applications. *Chem. Rev.* **1991**, *91*, 893–928.
34. Biegler-König, F.; Schnöbohm, J.; Bayles, D. AIM2000. *J. Comput. Chem.* **2001**, *22*, 545–559.
35. Biegler-König, F.; Schöbohm, J. Update of the AIM2000-Program for Atoms in Molecules. *J. Comput. Chem.* **2002**, *23*, 1489–1494.
36. Biegler-König, F. W.; Bader, R. F. W.; Tang, T. H. Calculation of the Average Properties of Atoms in Molecules. II. *J. Comput. Chem.* **1982**, *3*, 317–328.
37. Keith, T. A. AIMALL, Version 08.09.20 ed.; aim.tkgristmill.com, 2008.
38. Barlow, C. K.; Moran, D.; Radom, L.; McFadyen, W. D.; O'Hair, R. A. J. Metal-Mediated Formation of Gas-Phase Amino Acid Radical Cations. *J. Phys. Chem. A* **2006**, *110*, 8304–8315.
39. Ke, Y.; Zhao, J.; Verkerk, U. H.; Hopkinson, A. C.; Siu, K. W. M. Histidine, Lysine, and Arginine Radical Cations: Isomer Control via the Choice of Auxiliary Ligand (L) in the Dissociation of [Cu^{II}(L)(amino acid)]$^{\bullet 2+}$ Complexes. *J. Phys. Chem. B* **2007**, *111*, 14318–14328.
40. Gatlin, C. L.; Tureček, F.; Vaisar, T. Gas-Phase Complexes of Amino-Acids with Cu(II) and Diimine Ligands. 2. Amino-Aacids with O, N and S Functional-Groups in the Side-Chain. *J. Mass Spectrom.* **1995**, *30*, 1617–1627.
41. Boys, S. F.; Bernardi, F. Calculation of Small Molecular Interactions by Differences of Separate Total Energies: Some Procedures with Reduced Errors. *Mol. Phys.* **1970**, *19*, 553–566.

42. Ketvirtis, A. E.; Bohme, D. K.; Hopkinson, A. C. Theoretical Enthalpies of Formation of Compounds SiCH$_n$ (n = 0–4), SiC$_2$H$_n$ (n = 0–4, 6), SiCH$_n^+$ (n = 0–5), and SiC$_2$H$_n^+$ (n = 0–5, 7). *J. Phys. Chem.* **1995,** *99,* 16121–16127.

43. Steill, J.; Zhao, J.; Siu, C.; Ke, Y.; Verkerk, U. H.; Oomens, J.; Dunbar, R. C.; Hopkinson, A. C.; Siu, K. W. M. Structure of the Observable Histidine Radical Cation in the Gas Phase: A Captodative α-Radical Ion. *Angew. Chem. Int. Ed.* **2008,** *47,* 9666–9668.

44. Hopkinson, A. C.; Siu, K. W. M. In *Principles of Mass Spectrometry Applied to Biomolecules,* Laskin, J., Lifshitz, C., Eds.; Wiley–Interscience: New York, 2006; pp 301–335.

45. Hammerum, S. Distonic Radical Cations in Gaseous and Condensed Phase. *Mass Spectrom. Rev.* **1988,** *7,* 123–202.

46. Bordwell, F. G.; Zhang, X. M.; Alnajjar, M. S. Effects of Adjacent Acceptors and Donors on the Stabilities of Carbon-Centered Radicals. *J. Am. Chem. Soc.* **1992,** *114,* 7623–7629.

47. Easton, C. J. Free-Radical Reactions in the Synthesis of Alpha-Amino Acids and Derivatives. *Chem. Rev.* **1997,** *97,* 53–82.

48. Croft, A. K.; Easton, C. J.; Radom, L. Design of Radical-Resistant Amino Acid Residues: A Combined Theoretical and Experimental Investigation. *J. Am. Chem. Soc.* **2003,** *125,* 4119–4124.

49. Siu, C. K.; Ke, Y.; Guo, Y.; Hopkinson, A. C.; Siu, K. W. M. Dissociations of Copper(II)-Containing Complexes of Aromatic Amino Acids: Radical Cations of Tryptophan, Tyrosine, and Phenylalanine. *Phys. Chem. Chem. Phys.* **2008,** *10,* 5908–5918.